ACS APPLIED MATERIALS & INTERFACES

Research Article

www.acsami.org

Covalent cum Noncovalent Functionalizations of Carbon Nanotubes for Effective Reinforcement of a Solution Cast Composite Film

Wei Yuan and Mary B. Chan-Park*

School of Chemical and Biomedical Engineering, Nanyang Technological University, 62 Nanyang Drive, Singapore 637459, Singapore

Supporting Information

ABSTRACT: Although carbon nanotubes have impressive tensile properties, exploiting these properties in composites, especially those made by the common solution casting technique, seems to be elusive thus far. The reasons could be partly due to the poor nanotube dispersion and the weak nanotube/matrix interface. To solve this dual pronged problem, we combine noncovalent and covalent functionalizations of nanotubes in a single system by the design and application of a novel dispersant, hydroxyl polyimide-*graft*-bisphenol A diglyceryl acrylate (PI_{OH}-BDA), and use them with epoxidized single-walled carbon nanotubes (O-SWNTs). Our novel PI_{OH}-BDA dispersant functionalizes the nanotubes noncovalently to achieve good dispersion of the nanotubes because of the strong $\pi-\pi$ interaction due to main chain and steric hindrance of the BDA side chain. PI_{OH}-BDA also functionalizes O-SWNTs covalently because it reacts with epoxide groups on the nanotubes, as well as the cyanate ester (CE) matrix used. The resulting solution-cast CE composites show 57%, 71%, and 124% increases in Young's modulus, tensile strength, and toughness over neat CE. These values are higher than those of composites reinforced with pristine SWNTs, epoxidized SWNTs, and pristine SWNTs dispersed with PI_{OH}-BDA. The modulus and strength increase per unit nanotube weight fraction, i.e., dE/dW_{NT} and $d\sigma/dW_{NT}$, are 175 GPa and 7220 MPa, respectively, which are significantly higher than those of other nanotube/thermosetting composites (22−70 GPa and 140−3540 MPa, respectively). Our study indicates that covalent cum noncovalent functionalization of nanotubes is an effective tool for improving both the nanotube dispersion and nanotube/matrix interfacial interaction, resulting in significantly improved mechanical reinforcement of the solution-cast composites.

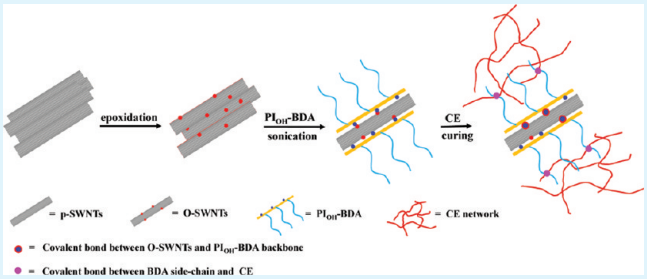

KEYWORDS: *single-walled carbon nanotubes, covalent functionalization, noncovalent functionalization, cyanate ester, mechanical properties*

INTRODUCTION

Carbon nanotubes (CNTs) are considered to be ideal reinforcement materials for high-performance lightweight polymer composites due to their combination of low density, large aspect ratio, and outstanding mechanical properties.[1−4] For example, Young's modulus and tensile strength of singled-walled carbon nanotubes (SWNTs) have been measured to be in the range of 0.32−1.47 TPa and 10−52 GPa, respectively.[5] However, pristine CNTs have limited solubility in either solvents or polymer matrixes due to their hydrophobicity and strong intertube van der Waals forces. Further, stress transfer between polymer matrix and the CNT filler is usually poor due to the smooth and hydrophobic graphene surface of CNTs. These two effects greatly hamper the reinforcement effect of CNTs in polymer composites.

To achieve good nanotube dispersion and strong nanotube/matrix interfacial adhesion, both covalent[6−8] and noncovalent[9−11] functionalization of CNTs have been reported. The most widely reported covalent approach is open-end functionalization through oxidant treatment[12−14] to form shortened CNTs with terminal carboxylic acid groups which can be further converted to other functional groups.[15,16] Another covalent approach is realized through sidewall reactions such as fluorination,[17] 1,3-dipolar cycloaddition,[18] reduction of diazonium salts,[19] and direct addition of radicals,[20] nitrenes,[21] and carbenes[22] to the unsaturated π system of nanotubes. Sidewall functionalization is effective for nanotube/matrix stress transfer because it better preserves the nanotube length, and higher concentration of sidewall functionalities is achievable. Though the covalent approach improves nanotube dispersion and nanotube/matrix interfacial strength, the covalent bonds inevitably disrupt the extended π conjugation of CNTs, leading to decreased electrical and mechanical properties of the resulting composites. Noncovalent functionalization, achieved by physical adsorption/wrapping of surfactants or polymers, has been shown to be highly effective at dispersing and debundling high concentrations of nanotubes in solvents and polymer matrixes without destruction of

Received: January 8, 2012
Accepted: March 20, 2012
Published: March 20, 2012

   dx.doi.org/10.1021/am300038d | ACS Appl. Mater. Interfaces 2012, 4, 2065−2073

Scheme 1. Preparation of CE Composites with SWNTs Functionalized by a Method That Combines Covalent and Noncovalent Approaches

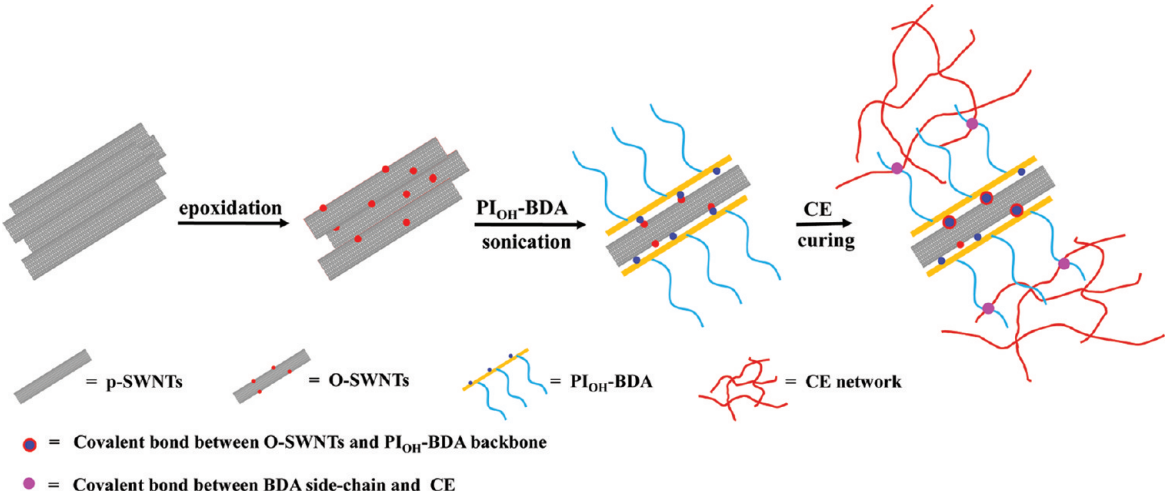

Scheme 2. (A) Sidewall Epoxidation of SWNTs. (B) Chemical Reaction between Epoxidized SWNTs and PI$_{OH}$-BDA

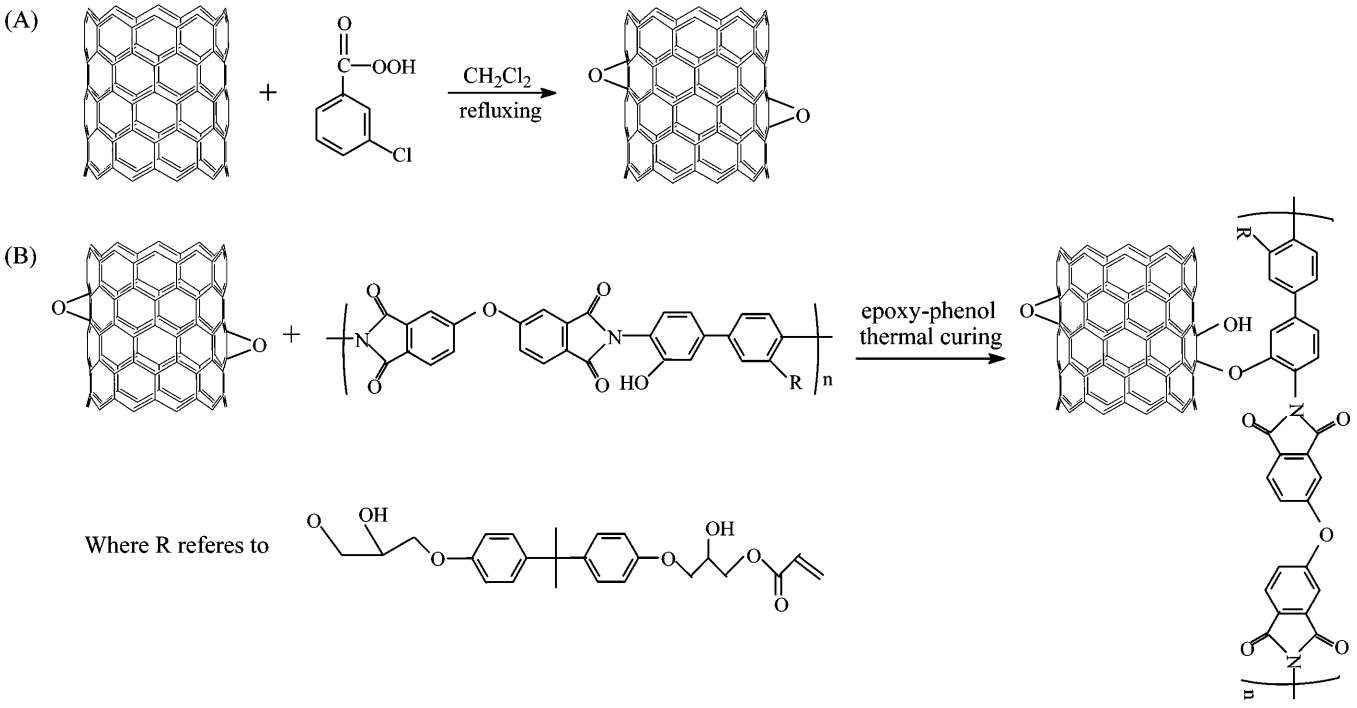

intrinsic nanotube structure. However, the noncovalent approach has a major drawback in that the interfacial strength between nanotubes and dispersant is usually relatively weak.

We hypothesize that nanotube functionalization by a combination of covalent and noncovalent approaches should result in improved enhancement of the composite mechanical properties. This combined approach, which has not previously been reported, requires a tailored reactive dispersant that effectively disperses the nanotubes and reacts with both the nanotube and matrix. For the nanotube−dispersant reaction, it is preferred that the functional groups be introduced on the sidewalls rather than the ends of CNTs for more effective stress transfer.

Cyanate esters (CEs) are a class of thermosetting resins with outstanding thermal and mechanical properties and have wide applications in the aerospace and electronics industries. One drawback of CEs is their brittleness due to the highly cross-linked network.[23] We and others have shown that addition of nanofillers, such as carbon nanotubes[24,25] and nanorod,[26] into CEs by solution casting is an effective approach for improving the toughness of CEs. These high-performance CNT/CE composites are believed to have wide applications in aerospace, defense, and transportation industries.

In this study, we report a novel nanotube functionalization method that combines covalent and noncovalent approaches for the reinforcement of CE matrix (Scheme 1). SWNTs were first covalently modified with epoxide groups on their sidewalls (Scheme 2A) and characterized by Raman, Fourier transform infrared (FT-IR), and thermogravimetric analysis (TGA) techniques. These epoxidized SWNTs (O-SWNTs) were dispersed by a reactive polymeric dispersant, hydroxyl polyimide-*graft*-bisphenol A diglyceryl acrylate (PI$_{OH}$-BDA),

dx.doi.org/10.1021/am300038d | ACS Appl. Mater. Interfaces 2012, 4, 2065−2073

and added into the CE to make composites by solution casting. During thermal curing, the phenolic hydroxyl groups in PI_{OH}-BDA backbone reacted with the epoxide groups on O-SWNTs (Scheme 2B) while the BDA side chains reacted with CE matrix, resulting in strong interfacial adhesion. CE composites were reinforced with pristine SWNTs (p-SWNTs); O-SWNTs and p-SWNTs dispersed with PI_{OH}-BDA (p-SWNTs/PI_{OH}-BDA) were also prepared. Nanotube dispersion, nanotube/matrix interfacial interaction, and mechanical properties of these four kinds of composites were investigated and compared. O-SWNTs/PI_{OH}-BDA was found to be the most effective filler for mechanical reinforcement of CE, which we interpret to be due to the superior dispersion of SWNTs and covalent nanotube/matrix interface.

EXPERIMENTAL SECTION

Materials. Chemical vapor deposition (CVD) method produced SWNTs with diameters of 1−2 nm, lengths of 5−30 μm, and a purity of ∼90% were supplied by Chengdu Research Institute of Organic Chemistry, China. To remove the impurities (e.g., amorphous carbon and metal particles), SWNTs were heated at 350 °C for 2 h under air atmosphere followed by refluxing in 6 M HCl solution overnight. α-Glycidyl terminated bisphenol A acrylate (GBA) was supplied as Ebecryl 3605 from UCB chemicals, Malaysia. It was freeze-dried at −55 °C for 48 h before use. 3-Chloroperoxybenzoic acid (*m*-CPBA, 77% max), 4-(dimethylamino) pyridine (DMAP, 99%), butylated hydroxytoluene (BHT, 99%), *N*,*N*′-dimethylformamide (DMF), dimethyl sulfoxide (DMSO), and dichloromethane (CH_2Cl_2) were purchased from Sigma-Aldrich. DMSO was distilled over calcium hydride, and all other chemicals were used as received. Bisphenol A cyanate ester resin was supplied by Shanghai Huifeng Technical & Business Co., Ltd. (China) with the trade name HF-1.

Synthesis of PI_{OH}-BDA. Polyimide backbone with pendant hydroxyl groups (PI) was first synthesized by a procedure described in our previous study.[25] To synthesize PI_{OH}-BDA, DMAP (0.293 g, 2.40 mmol) was added to a solution of PI (0.588 g, 1.20 mmol) in DMSO (40 mL) under argon protection. Then, a solution of GBA (0.594 g, 1.32 mmol) with BHT (0.018 g, 0.08 mmol) in DMSO (20 mL) was added. The mixture was reacted at 100 °C for 48 h under argon. The resulting solution was added dropwise into a large quantity of methanol (500 mL) to obtain PI_{OH}-BDA as a brown precipitate. The polymer was further purified by washing successively with 0.2 M HCl solution, 5 wt % $NaHCO_3$ solution, and DI water. The filter was dried at room temperature under vacuum for 48 h to afford 0.654 g (58% yield) of PI_{OH}-BDA.

Preparation of Epoxidized SWNTs (O-SWNTs). As shown in Scheme 2A, purified SWNTs (100 mg) were first added into CH_2Cl_2 (50 mL), and the mixture was sonicated in a sonicator bath (60 W, S30H, Elma) at 0 °C for 30 min. Then, the mixture was stirred at 50 °C for 48 h while at 12 h intervals a solution of *m*-CPBA (2.88 g, 16.5 mmol) in CH_2Cl_2 (50 mL) was added. After the reaction was complete, the mixture was filtered and washed several times with CH_2Cl_2 followed by methanol to remove any residuals. The resultant epoxidized SWNTs (O-SWNTs) powder was collected and dried under vacuum at 60 °C for 12 h.

Fabrication of SWNT/CE Composite Films. CE composite films reinforced with 1 wt % of carbon nanotubes were fabricated with four variations in the SWNT preparation: pristine SWNTs (p-SWNTs/CE), epoxidized SWNTs (O-SWNTs/CE), p-SWNTs dispersed with PI_{OH}-BDA (p-SWNTs/PI_{OH}-BDA/CE), and O-SWNTs dispersed with PI_{OH}-BDA (O-SWNTs/PI_{OH}-BDA/CE). A typical route used to fabricate p-SWNT/CE composite film was as follows: p-SWNTs suspension in DMF (1 mg/mL) was first prepared by sonication using a high-power tip sonicator (500 W, 35%, Vibra-Cell Sonics) for 10 min at 0 °C followed by 1 h sonication in a low-power bath sonicator (60 W, S30H, Elma). Then, a measured quantity of CE (partially cured at 180 °C for 1 h) solution in DMF (1 g/mL) was added into the nanotube suspension, and the mixture was sonicated in the bath sonicator for 10 min. Composite films were prepared by solution casting of this solution onto clean glass slides. Most of the solvent was removed by warming the slides on a hot plate at ∼50 °C for 6 h and further drying under vacuum at 80, 100, and 120 °C for 2 h each. Finally, the composite films were thermally treated successively at 180 °C for 3 h, 200 °C for 2 h, and 250 °C for 2 h under air to completely remove the solvent and achieve fully cured composites. O-SWNT/CE composites were prepared by a similar procedure using O-SWNTs instead of p-SWNTs. For fabrication of p-SWNTs/PI_{OH}-BDA/CE composite film, p-SWNTs/PI_{OH}-BDA dispersion was first prepared. Ten mg of p-SWNTs and 10 mg of PI_{OH}-BDA were added into 10 mL of DMF, and this mixture was sonicated with a tip sonicator for 10 min at 0 °C followed by sonication in a bath sonicator for 1 h. Then, a measured quantity of CE solution in DMF was added, and the mixture was sonicated in the bath sonicator for 10 min. Composite films were prepared by solution casting followed by thermal curing. O-SWNTs/PI_{OH}-BDA/CE composites were prepared by a similar route using O-SWNTs instead of p-SWNTs.

Characterization. ^{1}H NMR spectrum of PI_{OH}-BDA was recorded on a Bruker (300 MHz) NMR instrument using deuterated dimethylsulfoxide (DMSO-d_6) as solvent. Fourier transform infrared (FT-IR) spectra were obtained on a Nicolet 5700 FT-IR instrument. Pristine and functionalized SWNTs were dispersed in KBr pellets, and the spectra were obtained at a resolution of 4 cm^{-1} and were averaged over 64 scans. Thermogravimetric analysis (TGA) was conducted on a Netzsch STA 409 PG/PC machine under nitrogen with a heating rate of 10 °C/min and a temperature range of 50 to 800 °C. Raman spectra were recorded on a Renishaw Ramanscope with HeNe laser at an excitation wavelength of 633 nm. UV−vis−NIR absorption spectra of functionalized SWNT dispersions were obtained on a Varian Cary 5000 UV−vis−NIR spectrophotometer. Optical microscopy of composite films was conducted on an Olympus SZX12 microscope at a magnification of 144×. Atomic force microscopy (AFM) was performed on a MFP 3D microscope in ac mode. SWNT dispersions were spin-coated onto freshly cleaved silicon wafers. Transmission electron microscope (TEM) images were obtained on a JEOL 2100F high-resolution transmission electron microscope operated at 200 kV. TEM samples were prepared by dropping cast of O-SWNT/PI_{OH}-BDA dispersion onto a carbon-coated copper grid followed by solvent evaporation at room temperature. Field-emission scanning electron microscope (FE-SEM) images were acquired using a JEOL JSM-6700F microscope. The fractured surfaces of composite films were sputter-coated with a thin layer of gold prior to SEM observation. Tensile tests of composite films were performed on an Instron 5543 mechanical tester with a 100 N load cell at ambient temperature. The gauge length was 20 mm, and the crosshead speed was 2.54 mm/min. Mechanical properties of each composite formulation were measured on five to ten specimens, and property averages and standard deviations were computed.

RESULTS AND DISCUSSION

Synthesis of PI_{OH}-BDA Dispersant. In our previous study,[25] PI backbone was reacted with 2.2 equiv of GBA (i.e., polymer repeat units) to yield a polyimide graft with every pendant −OH group grafted with a side chain. In this study, PI backbone was reacted with 1.1 equiv of GBA under the same conditions to produce a new polyimide graft, PI_{OH}-BDA, in which 50% of the −OH groups were grafted with BDA side chain while the other 50% remained intact. The successful synthesis of PI_{OH}-BDA was confirmed by ^{1}H NMR spectrum (Figure 1). Characteristic peaks of aromatic protons and phenolic −OH group in polyimide backbone are present at δ 7.1−8.2 (b−g) ppm and δ 10.2 (a) ppm, respectively. The two sets of peaks at δ 6.7 (k) and 7.0 (l) ppm are attributed to the aromatic protons of the BDA side chain. Another three sets of peaks at δ 5.8 (s), 6.1 (q), and 6.2 (r) ppm are assigned to the −OCOCH=CH_2 terminal group. The aliphatic protons of −OCH and −OCH_2 of BDA side chain appear at δ 3.0−4.5 (h,

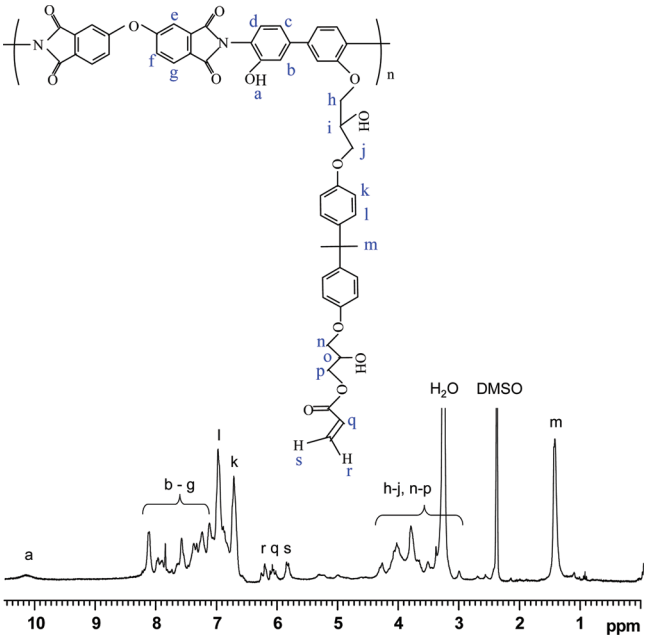

Figure 1. ^{1}H NMR spectrum of PI_{OH}-BDA.

i, j, n, o, and p) ppm, while those of $-CH_3$ groups are at δ 1.5 (m) ppm. The relative ^{1}H NMR integration ratio of $-CH_3$ peak to phenolic $-$OH peak is 5.7, indicating that about 50% of the $-$OH groups remain intact in the final PI_{OH}-BDA.

Preparation of Epoxidized SWNTs. The grafting of epoxide groups onto SWNTs using peroxide acid was realized via the method reported by Ogrin et al.[27] The effect of reaction time on the covalent sidewall functionalization was studied by Raman spectroscopy. As shown in Figure 2, the Raman spectra

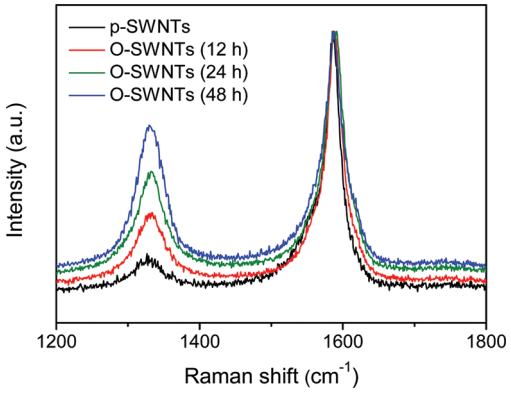

Figure 2. Raman spectra of p-SWNTs and O-SWNTs with reaction time of 12, 24, and 48 h.

of SWNTs show the typical disorder-induced mode (D-band) at ~1330 cm^{-1} and tangential mode (G-band) at ~1585 cm^{-1}. The intensity ratio of D-band to G-band (I_D/I_G) of p-SWNTs is about 0.1, while that of O-SWNTs obtained after reaction at 50 °C for 12, 24, and 48 h increased to 0.25, 0.4, and 0.58, respectively. The increase of I_D/I_G ratio after epoxidation, resulting from chemical disruption of sp^2 carbons in nanotube walls, indicates that the epoxide groups were covalently grafted onto the nanotube surface.[20,27,28] The progressive increase of the I_D/I_G ratio with reaction time indicates progressive introduction of defects onto the nanotube surface. It should be noted that our SWNTs are less reactive than the HiPco SWNTs used by Ogrin et al.[27] HiPco SWNTs showed a dramatic increase in the I_D/I_G ratio even when the reaction was conducted at room temperature for 12 h, while our SWNTs showed no obvious increase in the I_D/I_G ratio after reaction at room temperature for 48 h (data not shown). The higher reactivity of HiPco SWNTs may be due to their smaller diameter (~ 1 nm) and higher curvature.[29] For this reason, a higher reaction temperature (50 °C) was employed in the epoxidation of our larger diameter (1−2 nm) SWNTs.

The epoxidation of SWNTs was further confirmed by FT-IR spectra and TGA curves. As compared with the FT-IR spectrum of p-SWNTs (Figure 3, spectrum a), O-SWNTs

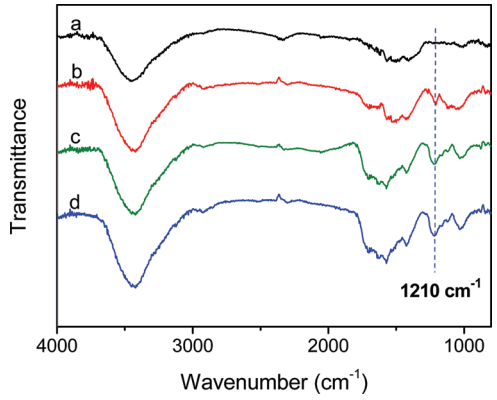

Figure 3. FT-IR spectra of (a) p-SWNTs and O-SWNTs with reaction time of (b) 12 h, (c) 24 h, and (d) 48 h.

with different reaction times all show a new absorption feature at 1210 cm^{-1} (Figure 3, spectrums b−d), which is characteristic of the epoxide moiety,[27,30] indicating that epoxide groups were successfully introduced to the nanotube surface. TGA curves (see Figure S1 in the Supporting Information) show that about 3, 8, and 14 wt % of epoxide groups were grafted to the surface of O-SWNTs with reaction time of 12, 24, and 48 h, respectively.

To make composites with high mechanical properties, a proper epoxidation time should be employed in order to balance the opposing requirements of (1) minimizing damage to the nanotube structure and (2) getting sufficient reaction sites on the nanotube sidewalls. To find out the optimal reaction time, 1 wt % of O-SWNTs with different reaction times (12, 24, and 48 h) were dispersed with PI_{OH}-BDA and added into CE to make cured composites. Mechanical property analysis (see Table S1 in the Supporting Information) shows that O-SWNT (24 h)/PI_{OH}-BDA/CE composites exhibit the highest tensile properties, indicating that 24 h is the optimal reaction time.

Dispersion of Nanotubes in DMF. DMF was chosen as solvent in this study because it not only dissolves PI_{OH}-BDA dispersant but also helps disperse carbon nanotubes.[31] The efficiency of DMF in dispersing CNTs can be attributed to its highly polar system and optimal geometries. Very recently, Alston et al.[32] directly measured the interaction between SWNTs and DMF using isothermal titration calorimetry. The dispersion of p-SWNTs, O-SWNTs, p-SWNTs/PI_{OH}-BDA, and O-SWNTs/PI_{OH}-BDA in DMF was first evaluated by visual observation. The results (see Figure S2 in the Supporting Information) show that O-SWNTs have better solubility than p-SWNTs in DMF due to the interaction between DMF solvent and the epoxide groups on the nanotube surfaces.[6] Both

p-SWNTs/PI_{OH}-BDA and O-SWNTs/PI_{OH}-BDA dispersions were homogeneously stable, and no precipitates were observed over 3 months of standing, which is apparently due to the noncovalent functionalization using PI_{OH}-BDA. The rigid aromatic backbone of the polyimide graft has strong $\pi-\pi$ interaction with the conjugated nanotube surface, while steric hindrance due to the pendant side chain located at the nanotube surface prevents nanotube reaggregation, leading to long-term stability of the dispersions.

A quantitative comparison of the solubility of p-SWNTs/PI_{OH}-BDA and O-SWNTs/PI_{OH}-BDA in DMF was performed by absorption spectra measurement. The nanotube concentration of a dispersion was determined from the Beer–Lambert law, $A = \varepsilon lc$, where A is the absorbance at a particular wavelength (here, we chose 500 nm), ε is the extinction coefficient (ε = 0.0376 L mg^{-1} cm^{-1} at 500 nm for our SWNTs in DMF[25]), l is the path length (l = 1 cm for our cell), and c is the nanotube concentration. p-SWNTs/PI_{OH}-BDA and O-SWNTs/PI_{OH}-BDA dispersions (mass ratio of SWNTs to polymer is 1:1) with initial nanotube concentration of about 20 mg/L were prepared. The absorbances of the initial solutions (20.0–20.1, Figure 4) and solutions subjected to different

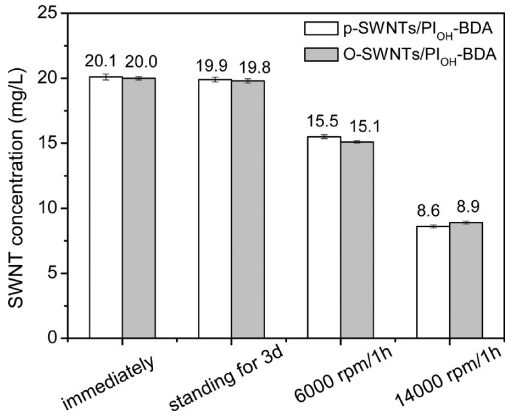

Figure 4. SWNT concentrations of p-SWNT/PI_{OH}-BDA and O-SWNT/PI_{OH}-BDA dispersions in different conditions: immediately after sonication, standing for 3 days, centrifugation at 6000 rpm for 1 h, and centrifugation at 14 000 rpm for 1 h.

sedimentation conditions were then measured. It was observed that, after standing for 3 days, centrifugation at 6000 rpm for 1 h, and centrifugation at 14 000 rpm for 1 h, the nanotube concentration of p-SWNTs/PI_{OH}-BDA decreased to 19.9, 15.5, and 8.6 mg/L, respectively, comparable to similar results for O-SWNTs/PI_{OH}-BDA (19.8, 15.1, and 8.9 mg/L, respectively) (Figure 4), indicating that p-SWNTs and O-SWNTs have similar solubility in DMF when dispersed with PI_{OH}-BDA. This observation suggests that the introduced epoxide groups on O-SWNTs do not affect the exfoliation of nanotubes which is realized by adsorption of PI_{OH}-BDA on the nanotube surface. The epoxidation process disrupts conjugated π system of nanotubes which may affect the $\pi-\pi$ interaction between PI_{OH}-BDA backbone and O-SWNTs, resulting in low solubility of O-SWNTs. However, the experimental results show that O-SWNTs do not have lower solubility than p-SWNTs when dispersed with PI_{OH}-BDA. We interpret this to be the effect of hydrogen bonding interaction between O-SWNTs and PI_{OH}-BDA, which also facilitates the adsorption of PI_{OH}-BDA onto O-SWNTs. The good affinity of PI_{OH}-BDA to O-SWNTs was also evidenced by TEM. As shown in Figure 5, there is clearly a layer of amorphous coating with nonuniform thickness on O-

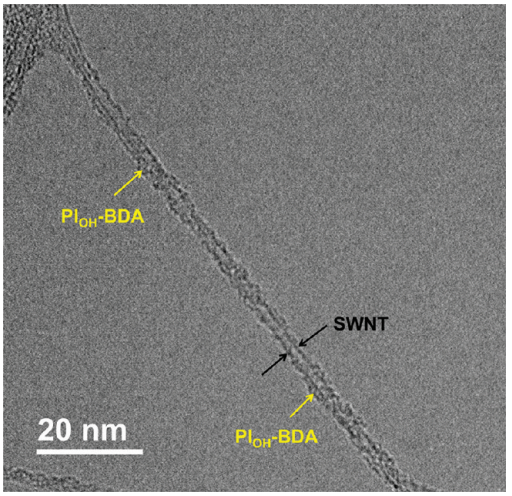

Figure 5. High-resolution TEM image of SWNTs/PI_{OH}-BDA.

SWNT surface, which is interpreted to be the adsorbed PI_{OH}-BDA.[10,33] FT-IR spectra (see Figure S3 in the Supporting Information) confirm that the interaction between PI_{OH}-BDA and O-SWNTs is so strong that not all PI_{OH}-BDA can be washed away by DMF. This result implies that it is reasonable to observe the adsorbed PI_{OH}-BDA layer on the nanotube surface under TEM.

The dispersion of p-SWNTs/PI_{OH}-BDA and O-SWNTs/PI_{OH}-BDA in DMF was further studied with AFM analysis. Figure 6 shows representative AFM images of p-SWNTs/PI_{OH}-BDA and O-SWNTs/PI_{OH}-BDA deposited on silicon wafers by spin coating. Both p-SWNTs and O-SWNTs can be dispersed well by PI_{OH}-BDA. The bundle sizes of both of the nanotubes are in the range of 1–3.5 nm, indicating that they are dispersed as individual tubes or as small bundles. The AFM images also show that O-SWNTs/PI_{OH}-BDA and p-SWNTs/PI_{OH}-BDA have similar lengths, implying that the epoxidation of SWNTs did not shorten the SWNTs. This is in contrast to acid treated SWNTs, which have shortened lengths and carboxyl groups mainly on the nanotube ends. The O-SWNTs with relatively long lengths and functional groups on the nanotube sidewalls are believed to be useful for mechanical reinforcement of polymer composites.

Nanotube Dispersion and Interfacial Bonding in Composites. The dispersion state of nanotubes in the four kinds of composite films was examined with optical microscopy and FE-SEM. The optical micrographs of p-SWNT/CE, O-SWNT/CE, p-SWNT/PI_{OH}-BDA/CE, and O-SWNT/PI_{OH}-BDA/CE composites are shown in Figure S4 in the Supporting Information. In p-SWNT/CE composites, nanotubes aggregate into large clusters with sizes of several tens of micrometers. O-SWNTs also form clusters in the CE matrix, but the cluster sizes are much smaller, indicating improved dispersion uniformity. In contrast, both p-SWNTs/PI_{OH}-BDA and O-SWNTs/PI_{OH}-BDA are dispersed uniformly throughout the matrix, and no obvious nanotube aggregates are present. These phenomena are consistent with the dispersibility of the four kinds of nanotubes in DMF.

To further evaluate the nanotube dispersion and nanotube/matrix interfacial bonding in composite films, fracture surfaces

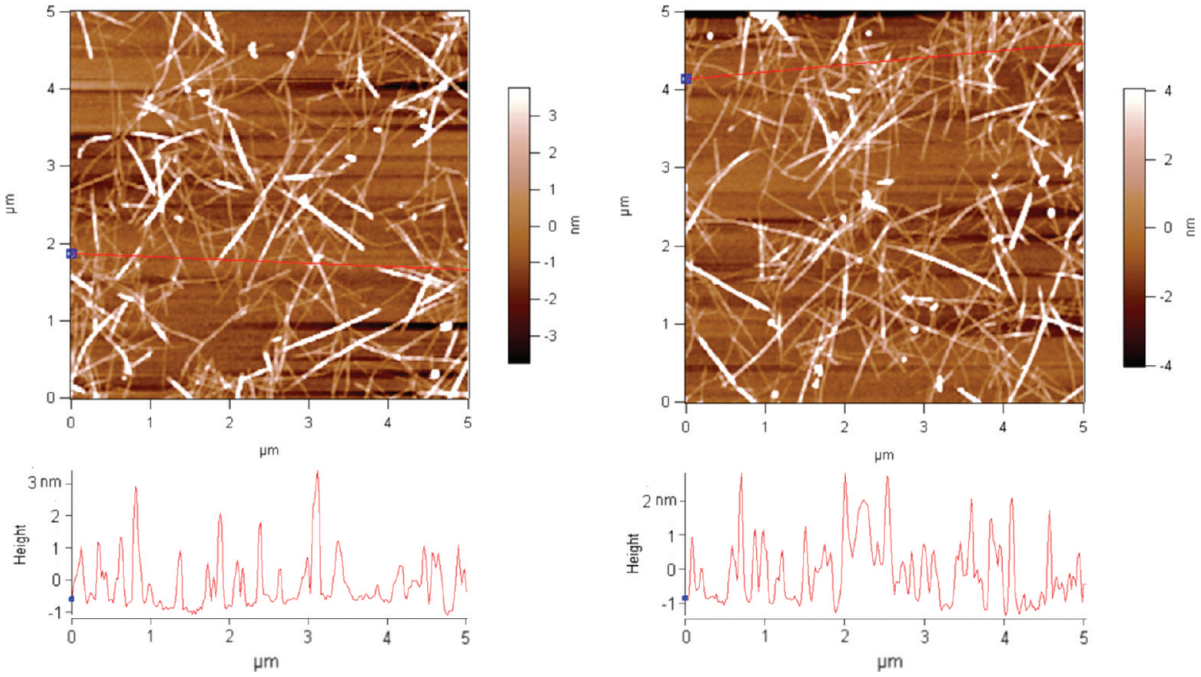

Figure 6. Typical AFM images of p-SWNTs/PI_{OH}-BDA and O-SWNTs/PI_{OH}-BDA spin-coated on silicon wafers.

of composites were examined with FE-SEM. The FE-SEM images of p-SWNT/CE composites (Figure 7A1−A3) show severe nanotube aggregation (indicated by circles in Figure 7A1) and many pulled-out nanotubes which indicate weak interaction between p-SWNTs and CE matrix. The nanotube dispersion in O-SWNT/CE composites (Figure 7B1−B3) is more homogeneous than that in p-SWNTs/CE, but nanotube aggregates with sizes of several hundreds of nanometers still can be clearly seen (Figure 7B1, circled). Some small bundles of O-SWNTs show only short tube ends on the surface, which indicate improved nanotube/matrix interfacial adhesion, resulting from the chemical reaction between the epoxide groups on O-SWNTs and the −OCN groups on CE.[34,35] The FE-SEM images of both p-SWNT/PI_{OH}-BDA/CE (Figure 7C1−C3) and O-SWNT/PI_{OH}-BDA/CE (Figure 7D1−D3) composites exhibit homogeneous dispersion of nanotubes. However, the pull-out length of nanotubes in O-SWNTs/PI_{OH}-BDA/CE is obviously shorter than that in p-SWNTs/PI_{OH}-BDA/CE, indicating stronger interfacial strength in O-SWNT/PI_{OH}-BDA/CE composites than in p-SWNT/PI_{OH}-BDA/CE composites.

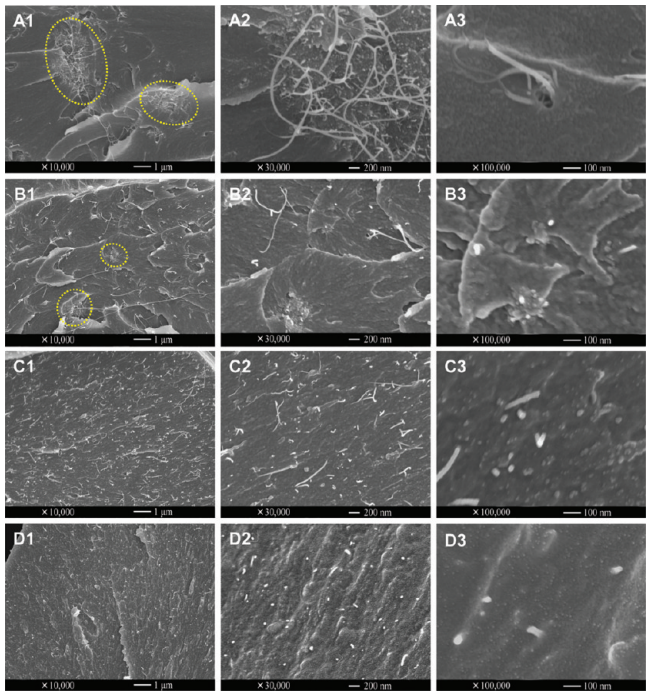

Figure 7. FE-SEM images of fracture surfaces of (A1−A3) p-SWNT/CE, (B1−B3) O-SWNT/CE, (C1−C3) p-SWNT/PI_{OH}-BDA/CE, and (D1−D3) O-SWNT/PI_{OH}-BDA/CE composites. Nanotube content is 1 wt %.

The strong interfacial adhesion in O-SWNT/PI_{OH}-BDA/CE composites can be attributed to three effects: (i) $\pi-\pi$ interaction between PI_{OH}-BDA backbone and conjugated nanotube surface; (ii) covalent bonding between epoxide groups on O-SWNTs and phenolic hydroxyl groups on the backbone of PI_{OH}-BDA (Scheme 2B); and (iii) chemical reaction between hydroxyl groups on the side chain of PI_{OH}-BDA and −OCN groups of CE. The interfacial adhesion in p-SWNT/PI_{OH}-BDA/CE composites is weaker because there is only noncovalent $\pi-\pi$ interaction but no chemical bonding between p-SWNTs and PI_{OH}-BDA backbone. The $\pi-\pi$ interaction and the reaction between PI_{OH}-BDA side chain and CE matrix have been proved in our previous study.[25] The reaction between O-SWNTs and phenolic hydroxyl groups was recently confirmed using FT-IR spectra by Cheng et al.[30] In our case, the absorption band of epoxide group (at 1210 cm^{-1}) is overlapped with the strong and broad band of C−O group (at 1230 cm^{-1}) of PI_{OH}-BDA, so FT-IR cannot be applied to study the reaction between O-SWNTs and PI_{OH}-BDA. To prove this reaction, O-SWNT/PI_{OH}-BDA mixture (mass ratio of 1:1) before and after the thermal curing process were washed with a large quantity of DMF by filtration and dried for TGA characterization (for details, see Figure S5 in the Supporting Information). The TGA shows that there is more PI_{OH}-BDA

Table 1. Mechanical Properties of Neat CE and Composites with 1 wt % of Nanotubes

sample	E (GPa)	σ (MPa)	ε (%)	T^a (MJ m^{-3})
neat CE	3.08 ± 0.14	101.1 ± 6.0	4.0 ± 0.3	2.1 ± 0.2
p-SWNTs/CE	3.25 ± 0.11 (6%)^b	66.2 ± 7.4 (−35%)	2.6 ± 0.5 (−35%)	0.9 ± 0.3 (−57%)
O-SWNTs/CE	3.31 ± 0.13 (8%)	90.7 ± 5.3 (−10%)	3.1 ± 0.3 (−23%)	1.5 ± 0.2 (−29%)
p-SWNTs/PI$_{OH}$-BDA/CE	3.83 ± 0.09 (24%)	132.6 ± 7.2 (31%)	5.0 ± 0.3 (25%)	3.8 ± 0.3 (81%)
O-SWNTs/PI$_{OH}$-BDA/CE	4.83 ± 0.15 (57%)	173.3 ± 8.9 (71%)	4.7 ± 0.4 (18%)	4.7 ± 0.4 (124%)

^{a}Calculated from the area under the stress−strain curve. ^{b}The values in brackets are increases of composite tensile properties over neat CE.

attached on the O-SWNT surface after the curing process, which is due to the covalent reaction between epoxide group of O-SWNTs and phenolic hydroxyl group of PI$_{OH}$-BDA.

Mechanical Properties. Table 1 lists the Young's modulus (E), tensile strength (σ), elongation at break (ε), and toughness (T) of neat CE and CE composites reinforced with 1 wt % of p-SWNTs, O-SWNTs, p-SWNTs/PI$_{OH}$-BDA, and O-SWNTs/PI$_{OH}$-BDA. Figure 8 shows their representative stress−strain

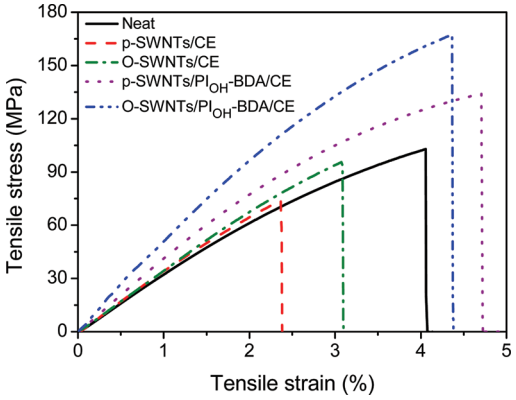

Figure 8. Representative stress−strain curves of neat CE and p-SWNT/CE, O-SWNT/CE, p-SWNT/PI$_{OH}$-BDA/CE, and O-SWNT/PI$_{OH}$-BDA/CE composites with nanotube loading of 1 wt %.

curves. The E, σ, ε, and T of neat CE are 3.08 ± 0.14 GPa, 101.1 ± 6.0 MPa, 4.0 ± 0.3%, and 2.1 ± 0.2 MJ m^{-3}, respectively, which are consistent with reported values.[23] Reinforcement with both p-SWNTs and O-SWNTs leads to a slight increase in Young's modulus but to decreases in tensile strength, elongation at break, and toughness. One wt% of p-SWNTs changes the E, σ, ε, and T by +6% (to 3.25 ± 0.11 GPa), −35% (to 66.2 ± 7.4 MPa), −35% (to 2.6 ± 0.5%), and −57% (to 0.9 ± 0.3 MJ m^{-3}) compared to the neat CE. The corresponding changes for O-SWNT/CE composite are +8% (to 3.31 ± 0.13 GPa), −10% (to 90.7 ± 5.3 MPa), −23% (to 3.1 ± 0.3%), and −29% (to 1.5 ± 0.2 MJ m^{-3}), respectively. The poor reinforcement effect of p-SWNTs and O-SWNTs is due to the nonuniform nanotube dispersion in CE matrix and relatively weak interaction between the nanotubes and the CE matrix. The higher reinforcement effect of O-SWNTs compared to p-SWNTs is due to the better nanotube dispersion in matrix and more efficient stress transfer at the interface, as discussed previously. Both p-SWNTs/PI$_{OH}$-BDA and O-SWNTs/PI$_{OH}$-BDA can improve the tensile properties of composites, but O-SWNTs/PI$_{OH}$-BDA is much more effective. The E, σ, ε, and T of p-SWNTs/PI$_{OH}$-BDA/CE composites increase to 3.83 ± 0.09 GPa, 132.6 ± 7.2 MPa, 5.0 ± 0.3%, and 3.8 ± 0.3 MJ m^{-3}, respectively, which are 24%, 31%, 25%, and 81% increases over that of neat CE. The corresponding values of O-SWNTs/PI$_{OH}$-BDA/CE composites are 4.83 ± 0.15 GPa, 173.3 ± 8.9 MPa, 4.7 ± 0.4%, and 4.7 ± 0.4 MJ m^{-3}, respectively, corresponding to increases of 57%, 71%, 18%, and 124% over neat CE. The elongation at break of O-SWNTs/PI$_{OH}$-BDA/CE is lower than that of p-SWNTs/PI$_{OH}$-BDA/CE composite, which is possibly due to the fact that the covalent bonds reduce nanotube pull-out (as observed in Figure 7) and restrict the nanotube network deformation during loading.[30]

It is quite attractive that 1 wt % of O-SWNTs/PI$_{OH}$-BDA is able to improve the toughness of CE by 124%. As discussed before, the brittleness of CEs often restricts their structural application. Our O-SWNT/PI$_{OH}$-BDA/CE composites with significantly improved toughness are believed to have wider applications as structural materials in industrial applications. We attribute the improved toughness to the homogeneously dispersed nanotubes, which have strong covalent bonding to the matrix and thus can effectively retard crack propagation during deformation.[24,26] The enhancement of Young's modulus and tensile strength of O-SWNT/PI$_{OH}$-BDA/CE composites is also significant when compared to other CNTs reinforced thermosetting resins.[4,6,8,36,37] For example, epoxy composites reinforced with 1 wt % of fluorinated SWNTs showed only 30% increase in Young's modulus and 14% increase in tensile strength.[6] The addition of 1 wt % of dendrimer-functionalized SWNTs into epoxy increased the Young's modulus and tensile strength by 26% and 17%, respectively.[37] To quantitatively evaluate the reinforcement effect of nanotubes, we calculated the variation of Young's modulus and tensile strength with nanotube weight fraction (dE/dW_{NT} and $d\sigma/dW_{NT}$).[8,25,38] The dE/dW_{NT} and $d\sigma/dW_{NT}$ of O-SWNT/PI$_{OH}$-BDA/CE composites are 175 GPa and 7220 MPa, respectively, which are more than twice the values of p-SWNT/PI$_{OH}$-BDA/CE composites (dE/dW_{NT} = 75 GPa and $d\sigma/dW_{NT}$ = 3150 MPa), indicating much higher reinforcement effect in CE of O-SWNTs/PI$_{OH}$-BDA than p-SWNTs/PI$_{OH}$-BDA. Furthermore, the mechanical improvement of O-SWNT/PI$_{OH}$-BDA/CE composites also compares favorably with the results of other CNT/thermosetting composites that have been reported recently, which showed dE/dW_{NT} of 22−70 GPa and $d\sigma/dW_{NT}$ of 140−3540 MPa.[8,25,39]

We attribute the excellent mechanical reinforcement in the O-SWNTs/PI$_{OH}$-BDA/CE composites to the good nanotube dispersion in the matrix and to strong chemical bonding at the nanotube/matrix interfaces, which are achieved via our method of combining covalent and noncovalent functionalization. As shown in Scheme 1, PI$_{OH}$-BDA adsorbs onto O-SWNT surface to disperse SWNTs into individual tubes or small bundles. Then, these O-SWNTs/PI$_{OH}$-BDA were added into CE to make composites. During thermal curing, the backbone of PI$_{OH}$-BDA reacts with the epoxide groups on O-SWNTs while the side chains of PI$_{OH}$-BDA react with the CE matrix, both of which lead to high interfacial adhesion between nanotubes and matrix. As a result, PI$_{OH}$-BDA, acting as both a nanotube

dispersant and a bonding agent between nanotubes and CE matrix, can effectively improve the Young's modulus, tensile strength, and toughness of composites. As discussed previously, the nanotube dispersion in p-SWNTs/PI_{OH}-BDA/CE and O-SWNTs/PI_{OH}-BDA/CE composites is quite similar (Figure 7), so the lower reinforcement effect of p-SWNTs/PI_{OH}-BDA to CE matrix is attributable to the weaker adhesion at the interface, which involves no covalent bonding between PI_{OH}-BDA backbone and p-SWNT surface.

CONCLUSIONS

We showed that covalent combined with noncovalent functionalizations of SWNTs synergistically improve the mechanical properties of the resulting solution-cast CE composite films. To effect the covalent cum noncovalent nanotube functionalizations, we have developed a novel dispersant, specifically PI_{OH}-BDA, which effectively disperses the SWNTs by noncovalent interaction and is also dual-functionalized so that it can react with O-SWNTs and CE to bridge the nanotube/matrix interface. The incorporation of 1 wt % of O-SWNTs/PI_{OH}-BDA into CE increases the Young's modulus, tensile strength, and toughness by 57%, 71%, and 124%, respectively. These values are much higher than those of control samples: CE composites reinforced with p-SWNTs (6%, −35%, and −57%, respectively), O-SWNTs (8%, −10%, and −29%, respectively), or p-SWNTs/PI_{OH}-BDA (24%, 31%, and 81%, respectively). The dE/dW_{NT} and $d\sigma/dW_{NT}$ of O-SWNT/PI_{OH}-BDA/CE composites are 175 GPa and 7220 MPa, respectively, which are significantly higher than reported values for other CNT/thermosetting composites. These dual functionalizations of the nanotubes effectively improve both nanotube dispersion and nanotube/matrix interfacial strength, leading to superior mechanical reinforcement in polymer composites. With appropriate modification of the side-chain chemistry of the CNT/matrix linking polymer, the dual covalent/noncovalent functionalization technique may be employed to improve SWNT reinforcement of other polymer or thermosetting materials.

ASSOCIATED CONTENT

Supporting Information

TGA curves of p-SWNTs and O-SWNTs; mechanical properties of CE composites reinforced with O-SWNTs; visual appearance of nanotube dispersions; FT-IR spectra of O-SWNTs, PI_{OH}-BDA, and O-SWNT/PI_{OH}-BDA complex; optical micrographs of nanotube/CE composites; TGA curves of washed O-SWNT/PI_{OH}-BDA mixture with and without thermal curing. This material is available free of charge via the Internet at http://pubs.acs.org.

AUTHOR INFORMATION

Corresponding Author

*Phone: +65 6316 8938. E-mail: mbechan@ntu.edu.sg.

Notes

The authors declare no competing financial interest.

ACKNOWLEDGMENTS

The authors gratefully acknowledge the financial support from the Defense & Science Technology Agency of Singapore (No. POD0513240) and Singapore National Research Foundation through a Competitive Research Program grant (NRF-CRP2-2007-02).

REFERENCES

(1) Moniruzzaman, M.; Winey, K. I. *Macromolecules* **2006**, *39*, 5194−5205.
(2) Coleman, J. N.; Khan, U.; Gun'ko, Y. K. *Adv. Mater.* **2006**, *18*, 689−706.
(3) Byrne, M. T.; Gun'ko, Y. K. *Adv. Mater.* **2010**, *22*, 1672−1688.
(4) Spitalsky, Z.; Tasis, D.; Papagelis, K.; Galiotis, C. *Prog. Polym. Sci.* **2010**, *35*, 357−401.
(5) Yu, M. F.; Files, B. S.; Arepalli, S.; Ruoff, R. S. *Phys. Rev. Lett.* **2000**, *84*, 5552−5555.
(6) Zhu, J.; Kim, J.; Peng, H.; Margrave, J. L.; Khabashesku, V. N.; Barrera, E. V. *Nano Lett.* **2003**, *3*, 1107−1113.
(7) Gao, J. B.; Itkis, M. E.; Yu, A. P.; Bekyarova, E.; Zhao, B.; Haddon, R. C. *J. Am. Chem. Soc.* **2005**, *127*, 3847−3854.
(8) Che, J.; Yuan, W.; Jiang, G.; Dai, J.; Lim, S. Y.; Chan-Park, M. B. *Chem. Mater.* **2009**, *21*, 1471−1479.
(9) Chen, J.; Ramasubramaniam, R.; Xue, C.; Liu, H. *Adv. Funct. Mater.* **2006**, *16*, 114−119.
(10) Zou, J. H.; Liu, L. W.; Chen, H.; Khondaker, S. I.; McCullough, R. D.; Huo, Q.; Zhai, L. *Adv. Mater.* **2008**, *20*, 2055−2060.
(11) Kim, K. H.; Jo, W. H. *Macromolecules* **2007**, *40*, 3708−3713.
(12) Chen, J.; Hamon, M. A.; Hu, H.; Chen, Y. S.; Rao, A. M.; Eklund, P. C.; Haddon, R. C. *Science* **1998**, *282*, 95−98.
(13) Banerjee, S.; Wong, S. S. *Nano Lett.* **2002**, *2*, 49−53.
(14) Hamon, M. A.; Chen, J.; Hu, H.; Chen, Y. S.; Itkis, M. E.; Rao, A. M.; Eklund, P. C.; Haddon, R. C. *Adv. Mater.* **1999**, *11*, 834−840.
(15) Ramanathan, T.; Fisher, F. T.; Ruoff, R. S.; Brinson, L. C. *Chem. Mater.* **2005**, *17*, 1290−1295.
(16) Kong, H.; Gao, C.; Yan, D. Y. *J. Am. Chem. Soc.* **2004**, *126*, 412−413.
(17) Mickelson, E. T.; Huffman, C. B.; Rinzler, A. G.; Smalley, R. E.; Hauge, R. H.; Margrave, J. L. *Chem. Phys. Lett.* **1998**, *296*, 188−194.
(18) Georgakilas, V.; Kordatos, K.; Prato, M.; Guldi, D. M.; Holzinger, M.; Hirsch, A. *J. Am. Chem. Soc.* **2002**, *124*, 760−761.
(19) Bahr, J. L.; Yang, J. P.; Kosynkin, D. V.; Bronikowski, M. J.; Smalley, R. E.; Tour, J. M. *J. Am. Chem. Soc.* **2001**, *123*, 6536−6542.
(20) Peng, H. Q.; Alemany, L. B.; Margrave, J. L.; Khabashesku, V. N. *J. Am. Chem. Soc.* **2003**, *125*, 15174−15182.
(21) Holzinger, M.; Abraha, J.; Whelan, P.; Graupner, R.; Ley, L.; Hennrich, F.; Kappes, M.; Hirsch, A. *J. Am. Chem. Soc.* **2003**, *125*, 8566−8580.
(22) Holzinger, M.; Vostrowsky, O.; Hirsch, A.; Hennrich, F.; Kappes, M.; Weiss, R.; Jellen, F. *Angew. Chem., Int. Ed.* **2001**, *40*, 4002−4005.
(23) Hamerton, I. *Chemistry and Technology of Cyanante Ester Resins*; Blackie Academic and Professional: London, 1994.
(24) Che, J. F.; Chan-Park, M. B. *Adv. Funct. Mater.* **2008**, *18*, 888−897.
(25) Yuan, W.; Feng, J. L.; Judeh, Z.; Dai, J.; Chan-Park, M. B. *Chem. Mater.* **2010**, *22*, 6542−6554.
(26) Pan, Y.; Xu, Y.; An, L.; Lu, H.; Yang, Y.; Chen, W.; Nutt, S. *Macromolecules* **2008**, *41*, 9245−9258.
(27) Ogrin, D.; Chattopadhyay, J.; Sadana, A. K.; Billups, W. E.; Barron, A. R. *J. Am. Chem. Soc.* **2006**, *128*, 11322−11323.
(28) Chen, Z.; Kobashi, K.; Rauwald, U.; Booker, R.; Fan, H.; Hwang, W. F.; Tour, J. M. *J. Am. Chem. Soc.* **2006**, *128*, 10568−10571.
(29) Rao, A. M.; Chen, J.; Richter, E.; Schlecht, U.; Eklund, P. C.; Haddon, R. C.; Venkateswaran, U. D.; Kwon, Y. K.; Tomanek, D. *Phys. Rev. Lett.* **2001**, *86*, 3895−3898.
(30) Cheng, Q. F.; Wang, B.; Zhang, C.; Liang, Z. Y. *Small* **2010**, *6*, 763−767.
(31) Landi, B. J.; Ruf, H. J.; Worman, J. J.; Raffaelle, R. P. *J. Phys. Chem. B* **2004**, *108*, 17089−17095.
(32) Alston, J. R.; Overson, D.; Poler, J. C. *Langmuir* **2012**, *28*, 264−271.
(33) Sinani, V. A.; Gheith, M. K.; Yaroslavov, A. A.; Rakhnyanskaya, A. A.; Sun, K.; Mamedov, A. A.; Wicksted, J. P.; Kotov, N. A. *J. Am. Chem. Soc.* **2005**, *127*, 3463−3472.
(34) Lin, C. H. *Polymer* **2004**, *45*, 7911−7926.

(35) Lin, C. H.; Yang, K. Z.; Leu, T. S.; Lin, C. H.; Sie, J. W. *J. Polym. Sci., Part A: Polym. Chem.* **2006**, *44*, 3487−3502.
(36) Zhu, J.; Peng, H. Q.; Rodriguez-Macias, F.; Margrave, J. L.; Khabashesku, V. N.; Imam, A. M.; Lozano, K.; Barrera, E. V. *Adv. Funct. Mater.* **2004**, *14*, 643−648.
(37) Sun, L.; Warren, G. L.; O'Reilly, J. Y.; Everett, W. N.; Lee, S. M.; Davis, D.; Lagoudas, D.; Sue, H. J. *Carbon* **2008**, *46*, 320−328.
(38) Coleman, J. N.; Khan, U.; Blau, W. J.; Gun'ko, Y. K. *Carbon* **2006**, *44*, 1624−1652.
(39) Yuan, W.; Li, W.; Mu, Y.; Chan-Park, M. B. *ACS Appl. Mater. Interfaces* **2011**, *3*, 1702−1712.